EVALUATION of DISPLACIVE MODELS for BAINITE TRANSFORMATION KINETICS in STEELS

María Jesús Santofimia[*1], Francisca G. Caballero, Carlos Capdevila, Carlos García-Mateo and Carlos García de Andrés.

Materalia Research Group, Department of Physical Metallurgy, Centro Nacional de Investigaciones Metalúrgicas (CENIM), Consejo Superior de Investigaciones Científicas (CSIC), Avda. Gregorio del Amo, 8. E-28040 Madrid, Spain

Synopsis

According to the displacive theory for bainite transformation, bainitic ferrite nucleates by the spontaneous dissociation of specific dislocation defects which are already present in the parent phase. The fact that the transformation stops well before equilibrium is achieved is consistent with a mechanism in which growth is diffusionless, although the

*1 Graduate Student, University of Cordoba, Spain. Present address: Materalia Research Group, Centro Nacional de Investigaciones Metalúrgicas (CENIM), Consejo Superior de Investigaciones Científicas (CSIC), Avda. Gregorio del Amo, 8. E-28040 Madrid, Spain.

carbon atoms are partitioned soon afterwards into the austenite from supersaturated ferrite. Cementite precipitation becomes possible when austenite carbon concentration exceeds the solubility limit given by the extrapolated $\gamma/\gamma+\theta$ phase boundary. These assumptions have led to several kinetics models for bainite transformation in steels that have been widely applied in industry and research. The majority of these models, that do not consider the effect of cementite precipitation during bainite transformation, were validated in high silicon bainitic steels in order to avoid the interference of cementite precipitation during bainite formation. In this work, displacive models for bainite transformation have been validated in bainitic steels with different silicon content with the aim of evaluating their applicability on steels where cementite precipitation may play an important role on bainite formation. It has been found that the reviewed models fail in the calculus of the maximum volume fraction of bainite of lean silicon steels, but lead to a reasonable accuracy in high silicon steels. This is not surprising since cementite formation reduces the carbon content in the residual austenite, stimulating the formation of a further quantity of ferrite. Likewise, an imprecise estimation of the nucleation rate of bainite must be the reason for the poor correlation in the predictions of the bainite transformation kinetics in high silicon steels. This entails a better treatment of autocatalytic nucleation, still unresolved issue in the bainite transformation kinetics theory.

Keywords: bainite, transformation kinetics, steels.

Abridged title: DISPLACIVE MODELS for BAINITE TRANSFORMATION

1. Introduction

Nowadays, there are two confronted theories of the kinetic of bainite transformation, based on reconstructive and displacive mechanisms, respectively. The former theory considers[1,2] that bainite is a non-lamellar two-phase aggregate of ferrite and carbides in which the phases form consecutively, as distinct from pearlite where they form cooperatively. According to this definition, the upper limiting temperature of bainite formation should be that of the eutectoid reaction (Ae_1), so the bainite start temperature, B_S, has not any fundamental significance. Thus, the bainitic 'bay' is the highest temperature in the range where the 'coupled solute drag effect' slows ferrite growth sufficiently so that growth can be increasingly supplemented by sympathetic nucleation, in agreement with the increasingly refined microstructure at 'sub-bay' temperatures[3,4]. The surface relief introduced as bainite growth is not clearly of invariant-plane strain (IPS) type for these authors, and some claim that relieves observed are tent-shaped[5,6]. In any case, models for the development of IPS and tent-shaped surface relieves have been published for difusional phase transformations, trying to explain the surface relieves observed in bainite from a reconstructive point of view[7].

By contrast, according to the displacive theory[8-10], the formation of bainite causes a deformation which is an IPS with a larger shear and a dilatational strain normal to the habit plane. This surface relief is considered an evidence of a martensitic mechanism of transformation.

Bainite nucleation is considered to occur by the spontaneous dissociation of specific dislocation defects which are already present in the parent phase, with the activation energy proportional to the driving force, as opposed to the inverse square relationship predicted by classical theory[11]. On the other hand, the lower C-curve in the temperature-time-transformation diagram is believed to have a characteristic flat top at a temperature T_h, which is the highest temperature at which ferrite can form by a displacive mechanism. The critical value of the chemical free energy change at T_h versus the value of T_h, is a straight line which led to a function G_N named 'universal nucleation function' which establishes a criterion for the nucleation of bainite. The form of G_N is given by:

$$G_N = C_1 T_h - C_2 \text{ J mol}^{-1} \quad (1)$$

where the units of T_h are in Kelvin and the values of the constants C_1 and C_2 are 3.5463 J/mol K and 3499.4 J/mol, respectively[11]. The subunit growth is considered diffusionless, although soon afterwards the excess of carbon is partitioned to the surrounded austenite, and stifled by the strength of the residual austenite[12,13]. Cementite can then precipitate from the enriched austenite between the ferrite plates. The process continues by successive nucleation of subunits until the carbon concentration of the residual austenite reaches the value at which the free energy of bainite becomes less than that of austenite of the same

composition, i.e. the T_0 curve[14-16] (or T_0', if the stored energy of ferrite is taken into account). This trend is known as 'incomplete reaction phenomenon' because the transformation ends before the carbon concentration of austenite reaches the equilibrium value[17].

In this work, kinetics models based on the assumptions of the displacive theory of bainite transformation are reviewed. These models that do not consider the effect of cementite precipitation during bainite transformation were experimentally validated in high silicon bainitic steels in order to avoid the interference of cementite precipitation during bainite formation. Here, bainite transformation kinetics results for steels with two different silicon contents have been used to validate and evaluate the applicability of these models on steels where cementite precipitation may play an important role on bainite formation.

2. Displacive Models for Isothermal Kinetics of Bainite Transformation

If no reaction overlaps with the bainite transformation and bainite formation continues until the carbon concentration of the residual austenite reach the T_0' curve, the maximum volume fraction of bainite that can be formed at a given temperature is estimated as follows[8,9]:

$$v_{\alpha B-\max} = \frac{x_{T_0^{'}} - \bar{x}}{x_{T_0^{'}} - x^{\alpha\gamma}} \tag{2}$$

where $x_{T_0^{'}}$ is the carbon concentration corresponding to the $T_0^{'}$ curve, $x^{\alpha\gamma}$ is the paraequilibrium carbon concentration of ferrite and $\bar{x}$ is the average carbon concentration of the alloy. Cementite precipitation in the residual austenite or inside bainitic ferrite forming lower bainite, should be taken into account in the calculations of $v_{\alpha B-\max}$. However, the majority of the existing displacive models do not considered the effect of cementite precipitation during bainite transformation. In fact, determination of the decrease in carbon content in the residual austenite or bainitic ferrite due to cementite formation has not been still well established[18].

Most of the reviewed models use the Johnson, Mehl, Avrami and Kolmogorov formulation (JMAK)[19] to estimate the volume fraction of bainite, $v_{\alpha B}$, formed in a time interval dt as follows:

$$dv_{\alpha B} = \left(1 - \frac{v_{\alpha B}}{v_{\alpha B-\max}}\right) dv_{\alpha B-ext} \tag{3}$$

where $dv_{\alpha B-ext}$ and $dv_{\alpha B}$ are the change of the bainite volume fraction in dt in the extended and real volume, respectively. Likewise, the time required to nucleate a ferrite sub-unit is considered to be much greater than that for its growth so bainite transformation is mainly controlled by the successive nucleation of subunits. Then, the extended volume of

bainite formed in dt is due to the number of subunits which nucleate in a given time interval:

$$dv_{\alpha B-ext} = uIdt \tag{4}$$

where u is the volume of a subunit and I is the nucleation rate per unit volume. Substituting in the expression of JMAK, it follows:

$$dv_{\alpha B} = \left(1 - \frac{v_{\alpha B}}{v_{\alpha B-\max}}\right) uIdt \tag{5}$$

Using a normalised fraction of bainite, $\xi_{\alpha B}$, defined as the volume fraction of bainite divided by the maximum volume fraction of bainite that can be formed:

$$\xi_{\alpha B} = \frac{v_{\alpha B}}{v_{\alpha B-\max}} \tag{6}$$

Equation (5) for the overall transformation kinetics is expressed as:

$$v_{\alpha B-\max} d\xi_{\alpha B} = \left(1 - \xi_{\alpha B}\right) uIdt \tag{7}$$

All the reviewed models in this work, except Matsuda and Bhadeshia model, coincide using this equation for the overall transformation kinetics. However, the main difference among all the evaluated models is related with the way of determining the nucleation rate.

2.1 Bhadeshia Model

Bhadeshia theory[20] for bainite transformation settled the basis of a set of models with analogous assumptions. In this sense, Bhadeshia model deserves a more in detail description.

This model considered that the growth of sheaves of bainite occurs by the martensitic propagation of bainitic ferrite subunits of a limited size *u*. A sub-unit nucleates at an austenite grain boundary and lengthens until its growth is arrested by plastic deformation within the austenite. New sub-units then nucleate at its tip, and the sheaf structure develops as this process continues.

The nucleation rate per unit volume, I , was described as:

$$I = B_1 \exp\left(-\frac{G^*}{RT}\right) \tag{8}$$

where R is the gas constant, B_1 is an empirical constant and G^* is the activation energy for nucleation involving the spontaneous dissociation of specific dislocation defects. The linear dependence of the activation energy on the driving force was substituted into the former nucleation rate equation to obtain:

$$I = B_1 \exp\left(-\frac{B_2 + B_3 \Delta G_m}{RT}\right) \tag{9}$$

where ΔG_m is the maximum driving force for nucleation, and B_2 and B_3 are constants.

At the highest temperature at which ferrite can form by displacive transformation, T_h, the maximum driving force for nucleation is equal to the universal nucleation function, G_N, and the nucleation rate at this temperature:

$$I_{T_h} = B_1 \exp\left(-\frac{B_2 + B_3 G_N}{RT_h}\right) \tag{10}$$

From equations (9) and (10), the nucleation rate could be expressed as:

$$I = I_{T_h} \exp\left(-\frac{B_2 \Delta T}{RTT_h} - \frac{B_3}{R}\left(\frac{\Delta G_m}{T} - \frac{G_N}{T_h}\right)\right) \tag{11}$$

where $\Delta T = T_h - T$.

The variation of ΔG_m with the extent of the reaction was considered[20]:

$$\Delta G_m = \Delta G_m^0 \left(1 - \frac{B_4}{B_3} \xi_{\alpha B} \cdot v_{\alpha B - \max} \right) \tag{12}$$

where B_4 is a constant and ΔG_m^0 is the initial driving force for nucleation.

In this model, Bhadeshia took into account the potential nucleation sites related to the autocatalysis phenomenon[21], introducing a dimensionless coefficient β in the determination of the nucleation rate as follows:

$$I_{T_h} = I_0 \left(1 + \beta \xi_{\alpha B} v_{\alpha B - \max} \right) \tag{13}$$

Thus, each plate of bainite creates new embryos in the austenite increasing the nucleation sites with the extent of transformation.

Analytical integration of the former equations led to four empirical constants: β, B_4, B_3 and B_2. For the determination of these empirical constants, experimental results on bainite transformation

kinetics for three steels were used. These steels, Fe-Mn-Si-C, Fe-Ni-Si-C and 300M, had high silicon content, so the formation of cementite in the residual austenite is suppressed, avoiding the interference of this reaction with bainite transformation kinetics. Chemical compositions of these steels are shown in Table 1, along with their corresponding prior austenite grain size (PAGS) for an austenitisation condition of 1000ºC for 300 s. The best fit values obtained by Bhadeshia for the different constants are shown in Table 2.

Transformation times predicted by the model were in reasonable agreement with experimental values. However, some systematic errors such as a small overestimation of the reaction rate at high temperatures and the underestimation of the effect of the alloying element on transformation results were detected. Later on, Rees and Bhadeshia[21)] confirmed this trend and proved that, contrary to experience, this model predicts faster bainite transformation kinetics in alloys with higher manganese content. Moreover, this model is not consistent with the fact that all the steels, according to the definition of G_N function, should have identically nucleation rate at T_h temperature. Bear in mind that the G_N function was justified with martensite nucleation theory assuming that I_{T_h} is the same for all the steels[11)]. Thus, comparing the universal nucleation function of two hypothetical steels A and B at their respective T_{hA} and T_{hB} temperatures:

$$G_{NA} = C_1 T_{hA} - C_2 \qquad (14)$$

$$G_{NB} = C_1 T_{hB} - C_2 \tag{15}$$

The ratio between both nucleation rates leads to the following expression:

$$\frac{I_{T_{hA}}}{I_{T_{hB}}} = \exp\left(\frac{(B_2 - B_3 C_2)(T_{hB} - T_{hA})}{R T_{hA} T_{hB}} \right) \tag{16}$$

Since $I_{T_{hA}} = I_{T_{hB}}$ it follows that $B_2 = B_3 C_2$. However, numerical values of these constants do not verify this condition (See Table 2).

On the other hand, the carbon enrichment of the austenite, calculated by equation (12), leads to the following ratio between two empirical constants B_4/B_3 = 2.98. Thus, $\Delta G_m > 0$ if $v_{\alpha B} > 0.34$, which is not reliable in most of the cases. In fact, bainite grows until the carbon of the residual austenite reach the value set by the $T_0^{'}$ curve, which is a function of the temperature and the chemical composition of the alloy. Finally, this model does not take into account the effect of the austenite grain size in the transformation kinetics. Furthermore, it is not considered the effect of temperature on the volume of the bainitic ferrite plates.

2.2 Rees and Bhadeshia Model

Rees and Bhadeshia[22] tried to solve some of the above mentioned problems in Bhadeshia model. In this sense, the nucleation rate of the bainitic ferrite at the T_h temperature was forced to be constant for all the steels. The linear dependence of the activation energy on the maximum driving force for nucleation was modified as follows:

$$G^* = B_2 + \frac{B_2}{C_2}\Delta G_m \tag{17}$$

and the nucleation rate was expressed as:

$$I = B_1 \exp\left(-\frac{B_2}{RT} - \frac{B_2 \Delta G_m}{C_2 RT}\right) \tag{18}$$

At T_h temperature, the maximum driving force for nucleation is equal to the universal nucleation function, G_N. Thus, using equations (18) and (1), it is verified that $I_{T_h} = B_1 \exp\left(-B_2 C_1 / C_2 R\right)$, an expression for the nucleation rate at T_h temperature independent of the material. Thus, Rees and Bhadeshia sorted out one of the inconsistent points of Bhadeshia model.

On the other hand, they also tried to correct the dependence of the maximum driving force for nucleation with the carbon content. In this sense, they proposed the following dependence with the volume fraction of bainite formed:

$$\Delta G_m = \Delta G_m^0 - \xi_{\alpha B}\left(\Delta G_m^0 - G_N\right) \tag{19}$$

Thus, clearly, at the beginning of transformation the maximum driving force for nucleation is equal to the initial driving force for nucleation, $\Delta G_m = \Delta G_m^0$, whereas the maximum driving force for nucleation, is equal to the universal nucleation function at the end of the transformation, $\Delta G_m = G_N$.

They also showed that the peak of carbon in the bainitic ferrite/austenite interface causes a local decrease on the driving force available for transformation. The process of successive nucleation in previously formed plates is thus inhibited, suggesting that the autocatalysis factor used in the kinetic model should be dependent on the carbon concentration in the steel. In this sense, Rees and Bhadeshia proposed the following expression for the autocatalysis factor:

$$\beta = \lambda_1\left(1 - \lambda_2 \bar{x}\right) \tag{20}$$

where λ_1 and λ_2 are empirical constants and $\bar{x}$ is the mean carbon concentration in the material.

Likewise, the nucleation rate in the austenite grain boundary was assumed to be proportional to the surface area of austenite grain boundaries per unit volume S_V. Since S_V varies linearly with $\bar{L}^{-1}$, where $\bar{L}$ is mean linear intercept of a series of random lines with the austenite grain boundaries, the effect of the austenite grain size on the nucleation rate was included in the constant B_1 of equation (18) as follows:

$$B_1 = \frac{1}{\bar{L} B'_1} \tag{21}$$

where B'_1 is another empirical constant.

The overall transformation kinetics is determined substituting equations (17-21) in equation (7). The resulting equation was analytically integrated leading again to four empirical constants: $B_1^{'}/u$, B_2, λ_1 and λ_2. Experimental results on bainite transformation kinetics of high silicon steels such as Fe-Mn-Si-C, Fe-Ni-Si-C and 300M were used for the determination of these empirical constants. Their corresponding values are shown in Table 3.

The described model led to a reasonable agreement between predicted and experimental values on bainite transformation kinetics in the three steels. Thus, the effects of alloying elements such as Mn on bainite

transformation kinetics as well as the amount of bainite formed at temperatures close to B_S temperature were accurately predicted. However, the values of the obtained empirical constants are very different in each steel (Table 3). This is especially disturbing in the case of steel Fe-Mn-Si-C, as the authors pointed out. In particular, B_2 varies some orders of magnitude from one alloy to another being theoretically independent of the chemical composition.

An additional difficulty is related to the autocatalysis phenomenon. Alloys in Table 3 are listing in an increasing order of carbon content (see Table 1). Thus, the λ_1, and therefore β, are found to increase with the carbon content of the alloy. This is not consistent with the original definition of the parameter β expressed in equation (20). Finally, the proposed dependence of the maximum driving force for nucleation with the volume fraction of bainite in equation (19) was not experimentally confirmed.

Later on, Chester and Bhadeshia[23] reported an error on the analytically solution of the overall transformation equation proposed by Rees and Bhadeshia. This was numerically sorted out in successive applications. Likewise, they found a accurate analytical solution of Rees and Bhadeshia's transformation equation. On the other hand, they estimated the width of bainitic plates, u_w, as a function of the transformation temperature by fitting experimental results from Chang[24]:

$$u_w = 0.001077(T + 273) - 0.2681 \quad (22)$$

Thus, the volume of the bainitic ferrite subunits was determined as:

$$u = u_w \cdot u_t \cdot u_l \quad (23)$$

where u_t and u_l are the thickness and length, respectively, of a bainitic ferrite subunit. Assuming a plate shaped, a value of 10 μm for both dimensions[25] was considered. With these corrections, the values for the empirical constants of Rees and Bhadeshia model are slightly modified as can be observed in Table 4, but the problems of this model remain unresolved.

2.3 Singh Model

Considering only nucleation at the austenite grain boundaries, the 'initial' nucleation rate per unit volume was calculated by Singh[26] as:

$$I^0 = N_V^0 \nu \exp\left(-\frac{G^*}{RT}\right) \quad (24)$$

where ν is an attempt frequency and N_V^0 is the initial density of nucleation sites which depends on the austenite grain size by using the mean linear intercept, $\overline{L}$, as:

$$N_V^0 = \frac{B_1^{''}}{\overline{L}\,\alpha_p} \tag{25}$$

being $B_1^{''}$ a constant and α_p a relationship between the volume, *u*, and the width of the subunits, u_w:

$$u = \alpha_p u_w^3 \tag{26}$$

On the other hand, every nucleated plate can promote the autocatalytic nucleation of β new plates. Thus, after a time, t, the nucleation site density increases as follows:

$$N_V^T = N_V^0 + \beta I^0 t \tag{27}$$

So the nucleation rate, including autocatalysis, is rewritten as:

$$I = N_V^T \nu \exp\left(-\frac{G^*}{RT}\right) \tag{28}$$

Using equation (24), it follows that:

$$I = I^0\left(1+\beta t \nu \exp\left(-\frac{G^*}{RT}\right)\right) \tag{29}$$

This model considers the activation energy for nucleation and the dependence of β with the mean carbon content as those proposed by Rees and Bhadeshia (See equation (17) and (20)). The driving force for nucleation, however, was assumed constant along the transformation, so no relationship with the extent of transformation was considered. Finally, Singh used a neural network model to estimate the width of the ferrite subunits[27,28] as a function of the strength of the residual austenite, the driving force for nucleation of ferrite and indirectly the temperature.

Analytical integration of the overall transformation equation proposed by Singh included four empirical constants: $B_1^{''}$, B_2, λ_1 and λ_2. Experimental results on the bainite transformation kinetics of the steels Fe-Mn-Si-C, Fe-Ni-Si-C and 300M along with data from Chang[24] were used to fit those empirical constants. See Table 5 for details.

Results sorted out some of the problems of Rees and Bhadeshia model. Calculation of the autocatalysis factor was consistent with the fact that this phenomenon is more unlikely as the steel carbon concentration increases. Moreover, the order of magnitude of β values well-match with a sheaf morphology. Finally, the values of the empirical constants $B_1^{''}$ and B_4 do not exhibit high changes from one alloy to another. Experimental validation of Singh model revealed an excellent agreement between predicted and experimental values on overall transformation kinetics of steels Fe-Ni-Si-C, Fe-Mn-Si-C and 300M, but not in the steels studied by Chang[24]. Singh attributed this disagreement to the aspect ratio between the width and the length of a plate, which is not constant for all the alloys.

2.4 Opdenacker Model

Opdenacker[29] reported some problems concerning the determination of the nucleation sites in Singh model. More in detail, the term $\beta I^0 t$ in equation (27) represents a change in the extended volume, N_V^{ext}. In this sense, it was necessary to take into account that the available volume for autocatalytic nucleation decreases with the extent of transformation. Thus, the following expression was proposed in this model for the estimation of the nucleation sites:

$$dN_V^T = (1-\xi)\beta I d\tau \tag{30}$$

and integrating:

$$N_V^T = N_V^0 \exp\left[\beta\nu \exp\left(-\frac{G^*}{RT}\right)\int_{\tau=0}^{\tau=t}(1-\xi)d\tau\right] \tag{31}$$

The autocatalysis factor calculated according to Singh model, with an order of magnitude of some units, proved to be more realistic than those in Rees and Bhadeshia model. However, the term $\beta\nu\exp\left(-{}^{G^*}\!/_{RT}\right)$ in equation (29) is about 15 orders of magnitude higher than unit. An autocatalysis contribution of this magnitude to the nucleation rate is not realistic. In this sense, Opdenacker[29)] suggested to substituted in equation (29) the term $\beta\nu\exp\left(-{}^{G^*}\!/_{RT}\right)$ by $\beta\xi_{\alpha B}\nu_{aB-\max}$. This adjustment led to a better correlation of the model, even for the case of slower kinetics at the beginning of bainite transformation. The model was validated on two high silicon steels and in a low silicon steel, giving reasonable results in all the cases, but fitting the empirical constants on the same data. Although this model improved the determination of the number of nucleation sites, the proposed adjustment was not completely justified.

2.5 Matsuda and Bhadeshia Model

Matsuda and Bhadeshia[30] developed a model for the prediction of the temporal evolution of the bainite volume fraction as a function of transformation temperature, chemical composition and austenite grain size. This transformation model takes into account bainite nucleation at austenite surfaces as well as the successive nucleation of subunits of bainitic ferrite in the subunits previously formed. Although, austenite grain boundaries were assumed to be the most potential nucleation site at the initial stages of transformation. The nucleation rates at austenite grain boundaries and at subunits were estimated with similar expressions than those proposed by Rees and Bhadeshia (See equation (18)). On the other hand, the growth rate of sheaves of bainite was determined from the ratio between the length of a subunit and the time passed between two successive nucleation events.

Although the time between two nucleation events at subunits is the same for all the bainitic ferrite subunits, it is not plausible that all the sheaves start at the same time and grow in the same way. This is why in this model it was assumed that the actual interval between successive subunits is Gaussian distributed with the mean of the calculated elapsed time and standard deviation of 1/6 of that.

For calculation, a test-plane parallel to the boundary and at a distance y away from it is considered. Particles nucleated in the grain boundary intercept with this test-plane under different extended areas. By the

integration of these areas as a function of *y*, the extended volume fraction of bainite was calculated. This overall transformation model led to four empirical constants that have been determined using experimental results of the steels Fe-Ni-Si-C and 300M. Results of the steel Fe-Mn-Si-C were not included in the validation because of the poor correlation between experimental values for the maximum volume fractions of bainite and those predicted by the incomplete reaction phenomenon. Unfortunately, it was not able to validate this model in this work. A more detailed description of this model would be required in order to validate it.

3. Materials and Experimental Procedures

Two steels with different silicon content have been selected to validate and evaluate the applicability of the reviewed models on steels where cementite precipitation may play an important role on bainite formation. Their actual chemical composition is given in Table 6. Steel A was supplied as 30 mm hot rolled square bar, whereas Steel B was supplied as 12 mm hot rolled strip. Dilatometric and metallographic analyses of bainite isothermal transformation have allowed the experimental validation of the reviewed displacive models for bainite transformation kinetics. An Adamel Lhomargy DT1000 high-resolution dilatometer has been used for that purpose[31)]. The heating and cooling devices of this dilatometer have been also used to study

previously the austenitisation condition of these steels. In this sense, cylindrical dilatometric test pieces of 3 mm in diameter and 12 mm in length were used to reveal grain boundaries by the thermal etching method[32]. For this purpose, a surface 2 mm in width was generated along the longitudinal axis of samples by polishing and finishing with 1μm diamond paste. Later on, samples were austenitised in vacuum (>1Pa) at 1200 ºC for 60 seconds in the case of the Steel A, and 300 seconds at 925ºC for Steel B. Subsequently samples were cooled down to room temperature at 1 ºC/s. These samples do not require metallographic preparation after heat treatment; the prior austenite grain boundaries are revealed without chemical etching. The average austenite grain size was measured using an image analyser. Table 7 shows the resulting mean linear intercept in microns for both steels.

Moreover, dilatometric samples of each steel were austenitized at temperatures listed in Table 7 and then isothermally transformed at temperatures ranging from 300 to 550 ºC for different times before quenching into water. Specimens were ground, polished and etched in 2% nital solution. Light Optical Microscopy (LOM) and Scanning Electron Microscopy (SEM) were used to examine the resulting microstructures. A Jeol JSM-6500F Field Emission Scanning Electron Microscope operating at 7 kV was employed for this purpose. The volume fraction of bainite was estimated by a systematic manual point-counting procedure on optical and scanning electron micrographs at low magnification[33]. A grid superimposed on the microstructure provides, after a suitable number of placements, an unbiased statistical estimation of the volume fraction of bainite.

Stereological errors for the values of the volume fraction of bainite correspond to the standard deviation of the measurement. In the case of Steel B, where the cementite precipitation from residual austenite is inhibited by the judicious use of silicon, the metallographic measurements of volume fraction bainite were corrected taking into account that the bainitic sheaves contain approximately 15% of film retained austenite[34].

The martensite start temperature (M_s) of each steel was measured by dilatometry. Dilatometric specimens were heated to 1200 ^{o}C (Steel A) or 925ºC (Steel B) and then rapidly cooled. Each dilatometric test was performed twice. The formation of martensite during cooling was detected by monitoring the fractional change in dilatation with temperature. Each dilatometric test was performed twice. Metallographic examination by LOM and SEM allowed to determine the bainite start temperature (B_S) and lower bainite start temperature (LB_S). Between both B_S and LB_S temperatures, upper bainite is formed. Table 8 shows the measured values of M_S, B_S and LB_S in Steels A and B.

During lower bainite formation there are two competing reactions which help to relieve the excess of carbon in the ferrite: the partitioning of carbon into the residual austenite and the precipitation of carbides in the bainitic ferrite. Both reactions interact since partitioning reduces the amount of carbon available for precipitation, and vice versa. In this sense, the use of transformation kinetic results for lower bainite will complicate the evaluation of the applicability of

the reviewed models. Thus, only transformation kinetic results for upper bainite have been used for that purpose.

Finally, quantitative X-ray analysis was used to determine the total volume fraction of retained austenite in the Steel B after the completion of the bainite transformation. For this purpose, 11x5x2 mm^3 samples were machined. After grinding and final polishing using 1 μm diamond paste, the samples were etched to obtain an undeformed surface. They were then step-scanned in a SIEMENS D 5000 X-ray diffractometer using unfiltered Cu K_α radiation. The scanning speed (2θ) was less than 0.3 degree/min. The machine was operated at 40 kV and 30 mA. The retained austenite content was calculated from the integrated intensities of (200), (220) and (311) austenite peaks, and those of (002), (112) and (022) planes of ferrite[35]. Using three peaks from each phase avoids biasing the results due to any crystallographic texture in the samples[36]. The carbon concentration in the austenite was estimated by using the lattice parameters of the retained austenite[37].

4. Results and Discussion

Figure 1 shows the microstructure obtained by complete transformation to upper bainite in Steels A and B. The resulting microstructures consist on sheaves of upper bainite, retained austenite and some martensite. As expected, cementite precipitation from residual austenite has not been avoided in the lean silicon steel, Steel

A (See Fig. 1(b)). Overall transformation kinetic results for this alloy will help to evaluate how cementite precipitation affects bainite transformation kinetics. Since the reviewed kinetics models do not take into account this reaction, those results will allow to validate the applicability of those models in low silicon steels. On the contrary, the precipitation of cementite during bainite transformation was suppressed in Steel B due to the high silicon content of the alloy. Silicon has very low solubility in cementite and greatly retards its growth from austenite. The carbon that is rejected from the bainitic ferrite enriches the residual austenite, thereby stabilising it down to room temperature. The sheaves of bainite in that case consist of plates of bainitic ferrite separated by carbon enriched films of austenite as Figure 1(d) illustrated.

Table 9 shows experimental values for the maximum volume fraction of bainite formed at different temperatures together with $v_{\alpha B-\max}$ values predicted according to $T_0^{'}$ curve[38,39] and equation (2) for both steels. For the lean silicon steel (Steel A), significant differences were obtained between predictions and experimental values for all the temperature tested. This is not surprising since cementite precipitation was not suppressed during bainite transformation. Cementite particles act as sinks of carbon, reducing the carbon content of the residual austenite in such a way that no incomplete reaction phenomenon is observed[40]. Likewise, this reduction of carbon in the residual austenite during the bainite transformation stimulates the formation of a further quantity of ferrite. Therefore, the $T_0^{'}$ curve concept and equation (2) are not suitable for the estimation of the maximum volume fraction of

bainite formed. The determination of the amount of carbon lost during cementite precipitation is essential for the calculation of $v_{\alpha B-\max}$ in lean silicon bainitic steels.

On the other hand, predictions of $v_{\alpha B-\max}$ for Steel B were found lower than the corresponding experimental values. These differences must be related to a possible disagreement between the actual carbon content in the austenite and the $T_0^{'}$ curve. The carbon concentrations of the austenite determined from X-ray analysis are presented in Figure 2 together with the $T_0^{'}$ curve of Steel B. The measured concentration of austenite at the termination of upper and lower bainite reaction is closer to the $T_0^{'}$ value boundary and far from the paraequilibrium phase boundary. This is consistent with the ferrite growth mechanism without substitutional diffusion and with excess carbon partitioning into austenite after the formation of ferrite subunit. That is not the case for Widmanstätten ferrite, formed at 475 ºC in this steel, whose growth involves carbon diffusion under paraequilibrium as experimental results in Figure 2 suggests. The fact that the measured carbon concentrations of the austenite at the termination of bainite reaction exceed the $T_0^{'}$ concentration is a consequence of the fact that the isolated films of austenite between the bainite plates can accumulate carbon, beyond $T_0^{'}$[14]. They cannot, of course, transform to bainite once the $T_0^{'}$ curve is exceeded.

Figure 3 shows comparison of experimental and calculated results for the overall transformation kinetics of upper bainite in Steels A and B. In this figure, Rees and Bhadeshia[22] model revised by Chester[23],

Singh model[26] and Opdenacker model[29] are evaluated. The three models predict the evolution of the volume fraction of the bainite formed with time at a given temperature as a function of the chemical composition and the prior austenite grain size. The disagreement on $v_{\alpha B-\max}$ calculations presented in Table 9 makes necessary here the use of normalised kinetics curves, such as those presented in Figure 3, for the validation of the reviewed models. Although they are also affected by the lack of precision in the prediction of $v_{\alpha B-\max}$ values, normalised transformation curves allow us to understand and evaluate these modelling kinetics results.

According to Figure 3, the three models predict slower kinetics for upper bainite formation in Steel A than that derived from the experimental results. This is particularly significant in the case of Chester model (See Figure 3(a)). Likewise, it was not possible using Chester model to predict overall transformation results at 525 ºC in Steel A since this temperature is above the calculated B_s temperature (512 ºC) of this steel. Only kinetics results at 525 ºC from Singh model seems to predict the experimental results with a reasonable agreement. However, bearing in mind the significant deviation between predictions and experimental $v_{\alpha B-\max}$ values at this temperature (Table 9), no conclusions can be derived from this success. In fact, the predictions of the three models are affected by the disagreement on the calculation of $v_{\alpha B-\max}$ results. This value is iteratively used in the calculation of the overall transformation kinetics (See equation (7) as example). The underestimation of $v_{\alpha B-\max}$ value in Steel A leads to slow kinetics predictions for upper bainite formation in this steel. The

described situation is a consequence of cementite precipitation between bainitic ferrite plates. The precipitation of cementite reduces the carbon concentration in the residual austenite enhancing the formation of a further quantity of bainitic ferrite and thus speeding bainite transformation kinetics.

On the contrary, the reviewed models predict faster transformation kinetics in the high silicon steel (Steel B). An imprecisely estimation of the nucleation rate of bainite in the calculus must be the reason for the poor correlation in the predictions of the bainite transformation kinetics in this steel. In particular, the three models use an autocatalysis factor with similar expression and dependencies. A better understanding of the role of the autocatalytic nucleation in the bainite transformation is necessary for an improvement of the mathematical implementation of this phenomenon in the models. This entails a better treatment of autocatalytic nucleation, still unresolved issue in the bainite transformation kinetics theory.

6. Conclusions

Displacive models for bainite transformation have been reviewed and evaluated in bainitic steels with different silicon content. Models fail in the calculus of the maximum volume fraction of bainite of the lean silicon steel, but lead to a reasonable correlation in the high silicon steel. This is not surprising since cementite formation reduces the

carbon content in the residual austenite, stimulating the formation of a further quantity of ferrite. This explains the slow kinetics results predicted for bainite formation in the lean silicon steel.

On the contrary, models predict faster transformation kinetics in the high silicon steel. An imprecisely estimation of the nucleation rate of bainite in the calculus must be the reason for this poor correlation. This entails a better treatment of autocatalytic nucleation, still unresolved issue in the bainite transformation kinetics theory.

7. Acknowledgement

The authors acknowledge financial support from the European Coal and Steel Community (ECSC agreement number 7210-PR/345) and the Spanish Ministerio de Ciencia y Tecnología (Project-MAT 2002-10812 E) and from M.J. Santofimia would also like to express her gratitude to Consejo Superior de Investigaciones Científicas (CSIC) for the financial support in the form of a PhD Research Grant (I3P Program).

8. References

1) H. I. Aaronson: *The Decomposition of Austenite by Diffusional Processes,* ed. V. F . Zackary and H. I. Aaronson (Interscience Publishers, New York, 1962) pp. 387-546.

2) H. I. Aaronson: *The Mechanism of Phase Transformations in Crystalline Solids,* (The Institute of Metals, London, 1969) pp. 270-281.

3) H. I. Aaronson, G. Spanos and W. T. Reynolds Jr: Scr. Mater. **47** (2002) 139-144.

4) W. T. Reynolds Jr., F. Z. Li., C. K. Shui and H. I. Aaronson: Metall. Trans. A 21 (1990) 1433-1463.

5) H. S. Fang, X. Z. Bo and J. J. Wang: Mater. Trans. **39** (1998) 1463-1470.

6) H. I. Aaronson, J. M. Rigsbee, B. C. Muddle and J. F. Nie: Scr. Mater. **47** (2002) 207-212.

7) J. P. Hirth, G. Spanos, M. G. Hall and H. I. Aaronson: Acta Mater. **46** (1998) 857-868.

8) H. K. D. H. Bhadeshia: Acta Metall. **29** (1981) 1117-1130.

9) H. K. D. H. Bhadeshia and D. V. Edmonds: Acta Metall. **28** (1980) 1265-1273.

10) H. K. D. H. Bhadeshia: Scr. Metall. **14** (1980) 821-824.

11) C. Garcia-Mateo, H. K. D. H. Bhadeshia: Mater. Sci. Eng. A **378** (2004) 289-292.

12) H. K. D. H. Bhadeshia and J. W. Christian: Metall. Trans. A **21** (1990) 767-97.

13) S. B. Singh, H. K. D. H. Bhadeshia: Mater. Sci. Eng. A **12** (1996) 610-612.

14) H. K. D. H. Bhadeshia and A. R. Waugh: Acta Metall. **30** (1982) 775-784.

15) L. C. Chang and H. K. D. H. Bhadeshia: Mater. Sci. Eng. A **184** (1994) L17-L20.

16) I. Stark, G. D. Smith and H. K. D. H. Bhadeshia: *Solid-Solid Phase Transformations*, ed. by G. W. Lorimer (Institute of Metals, London, 1988) pp. 211-215.

17) H. K. D. H. Bhadeshia: *Proc. of the Int. Solid-Solid Phase Transformations Conference*, (The Metall. Soc. of the A.I.M.E., Pittsburgh, 1981) pp. 1041-1048.

18) H. K. D. H. Bhadeshia: Mater. Sci. Eng. A **273-275** (1999) 58-66.

19) J. W. Christian: *Theory of Transformations in Metals and Alloys*, Part 1, 2nd. ed., (Pergamon Press, Oxford, 1975) pp. 15-20.

20) H. K. D. H. Bhadeshia : Journal de Physique IV France **43** (1982) Colloque C4, 443-448.

21) H. K. D. H. Bhadeshia: *Bainite in Steels*, 2nd Ed. (The Institute of Materials, London, 2001) pp. 42-44.

22) G. I. Rees and H. K. D. H. Bhadeshia: Mater. Sci. Technol. **8** (1992) 985-993.

23) N. A. Chester and H. K.D. H. Bhadeshia: Journal de Physique IV France **7** (1997) Colloque C5, 41-46.

24) L. C. Chang: *Bainite Transformation and Novel Bainitic Rail Steels*, Ph.D. Thesis, (University of Cambridge, Cambridge, UK, 1995).

25) R. W. K. Honeycombe, H. K. D. H. Bhadeshia: *Steels. Microstructure and Properties*. (2nd. ed., Butterworth-Heinemann, Oxford, 2000) pp. 115-119.

26) S. B. Singh: *Phase Transformations from Deformed Austenite*, Ph.D. Thesis, (University of Cambridge, Cambridge, UK, 1998).

27) S. B. Singh and H. K. D. H. Bhadeshia: Mater. Sci. Eng. A **245** (1998) 72-79.

28) S. B. Singh and H. K. D. H. Bhadeshia: Materials Algorithms Project, http://www.msm.cam.ac.uk/map/neural/programs/plate-b.html.

29) P. Opdenacker: *The Rate of the Bainite Transformation*, Ph.D. Thesis, (University of Cambridge, Cambridge, UK, 2001).

30) H. Matsuda and H. K. D. H. Bhadeshia: Proc. R. Soc. London A **460** (2004) 1707-1722.

31) C. García de Andrés, F. G. Caballero, C. Capdevila and L. F. Álvarez: Mater. Charact. 48 (2002) 101-111.

32) C. García de Andrés, M. J. Bartolomé, C. Capdevila, D. San Martín, F. G. Caballero, V. López and J. Vara: Rev. Met. Madrid **37** (2001) 528-539.

33) G. F. Vander Voort: *Metallography. Principles and Practice*, (McGraw-Hill Book Company, New York, U.S.A., 1984) pp.426-428.

34) H. K. D. H. Bhadeshia and D. V. Edmonds: Metal Sci. **17** (1983) 411-419.

35) J. Durnin and K. A. Ridal: J. Iron Steel Inst. **206** (1968) 60-67.

36) M. J. Dickson: J. Appl. Cryst. **2** (1969) 176-180.

37) D. J. Dyson and B. Holmes: J. Iron Steel Inst. **208** (1970) 469-474.

38) H. K. D. H. Bhadeshia: Metal Sci. **16** (1982) 159-165.

39) H. K. D. H. Bhadeshia: Materials Algorithms Project, http://www.msm.cam.ac.uk/map/steel/programs/mucg73-b.html.

40) P. Jacques, E. Girault, T. Catlin, N. Geerlofs, T. Kop, S. van der Zwaag and F. Delannay: Mater. Sci. Eng. A **273-275** (1999) 475-479.

Number of letters and words

Letters: 32236

Words: 5930

List of captions of tables and Figures

Figure 2 Calculated $T_0^{'}$ and paraequilibrium Ae3 curves[39] for Steel B and experimental data for carbon composition of retained austenite at the termination of bainite and Widmanstätten reactions.

Figure 3 Comparison of experimental and calculated results for the overall transformation kinetics of upper bainite in Steels A and B. Reviewed models: a) and b) Chester and Bhadeshia[23] model; c) and d) Singh model[26]; and e) and f) Opdenacker model[29].

Tables and Figures

Table 1 Chemical composition in mass% and prior austenite grain size (PAGS) of the steels used by Bhadeshia for the development of its model [20, 22-23, 26, 30].

Steel	C	Si	Mn	Ni	Mo	Cr	V	PAGS/μm
Fe-Mn-Si-C	0.22	2.03	3.00	0.00	0.00	0.00	0.00	47 ± 5
Fe-Ni-Si-C	0.39	2.05	0.00	4.08	0.00	0.00	0.00	52 ± 6
300M	0.44	1.74	0.67	1.85	0.83	0.39	0.09	86 ± 9

Table 2 Best fit values for the empirical constants of Bhadeshia model using combined data from the steels Fe-Mn-Si-C, Fe-Ni-Si-C and 300M.

B_2 / J*mol^{-1}	B_3	B_4	β
2.9710*10^4	3.769	11	200

Table 3 Best fit values for the empirical constants of Rees and Bhadeshia model.

	$\frac{B'_1}{u}$ /m^{-1} s	B_2 / J mol^{-1}	λ_1	λ_2
Fe-Mn-Si-C	3.876*10^7	1.925	4.756	0.00
Fe-Ni-Si-C	2.028*10^7	2.907*10^4	90.822	0.00
300M	1.231*10^7	3.767*10^4	141.66	0.00
Combined data	3.390*10^7	2.065*10^4	139.00	25.46

Table 4 Best fit values for the empirical constants of Chester and Bhadeshia model using combined data from the steels Fe-Mn-Si-C, Fe-Ni-Si-C and 300M.

$\frac{B'_1}{u}$ /m^{-1} s	B_2 / J mol^{-1}	λ_1	λ_2
$3.4456*10^7$	$2.098*10^4$	147.50	30.327

Table 5 Best fit values for the empirical constants of Singh model.

	B''_1, m^{-2}	B_2, J mol^{-1}	λ_1	λ_2
Fe-Mn-Si-C	$3.845*10^{-25}$	$4.469*10^{4}$	2.203	0.00
Fe-Ni-Si-C	$1.945*10^{-25}$	$8.407*10^{4}$	1.865	0.00
300M	$2.432*10^{-25}$	$7.147*10^{4}$	1.416	0.00
Combined data. Including Chang's data	$3.845*10^{-25}$	$3.805*10^{4}$	4.932	45.158

Table 6 Chemical compositions of the studied steels in mass%.

Steel	C	Si	Mn	Ni	Mo	Cr	V	Al	Ti	S
A	0.31	0.25	1.22	0.10	0.03	0.14	0.004	0.00	0.00	0.01
B	0.29	1.48	2.06	0.006	0.265	0.43	0.00	0.008	0.002	0.00

Table 7 Austenitisation conditions and mean linear intercept measurements.

Steel	Austenitisation conditions	Mean linear intercept, $\overline{L}$ /μm
A	1200ºC - 60s	39 ± 14
B	925ºC - 300s	12 ± 5

Table 8 Experimental values of B_S, LB_S and M_S temperatures

Steel	B_S / ºC	LB_S / ºC	M_S / ºC
A	537 ± 12	462 ± 12	342 ± 4
B	462 ± 12	412 ± 12	364 ± 10

Table 9 Measurements and calculated values of the maximum volume fraction of upper bainite formed in both steels.

Steel		Maximum volume fraction of bainite				
		425ºC	450ºC	475ºC	500ºC	525ºC
A	Experimental	*Lower bainite*	*Lower bainite*	*Fully bainitic*	*Fully bainitic*	*Fully bainitic*
	Predicted	---	---	0.32	0.20	0.03
B	Experimental	0.53 ± 0.05	0.40 ± 0.05	*Widmanstätten ferrite*	*Widmanstätten ferrite*	*Widmanstätten ferrite*
	Predicted	0.40	0.27	---	---	---

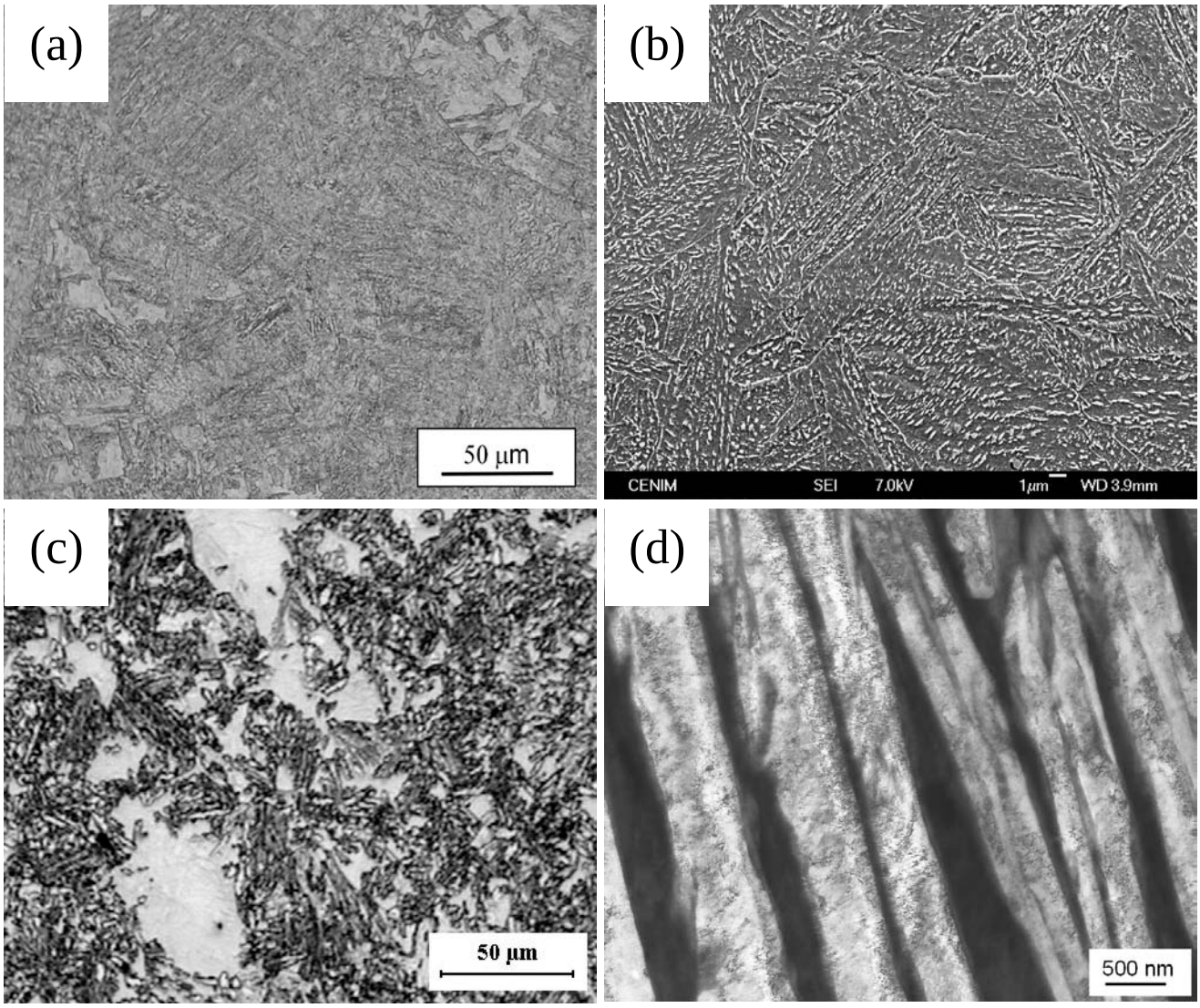

Figure 1 Optical and electron micrographs of microstructures obtained by isothermal transformation: (a) and (b) at 475ºC for 1800s in Steel A; (c) and (d) at 425 ºC for 1800 s in Steel B.

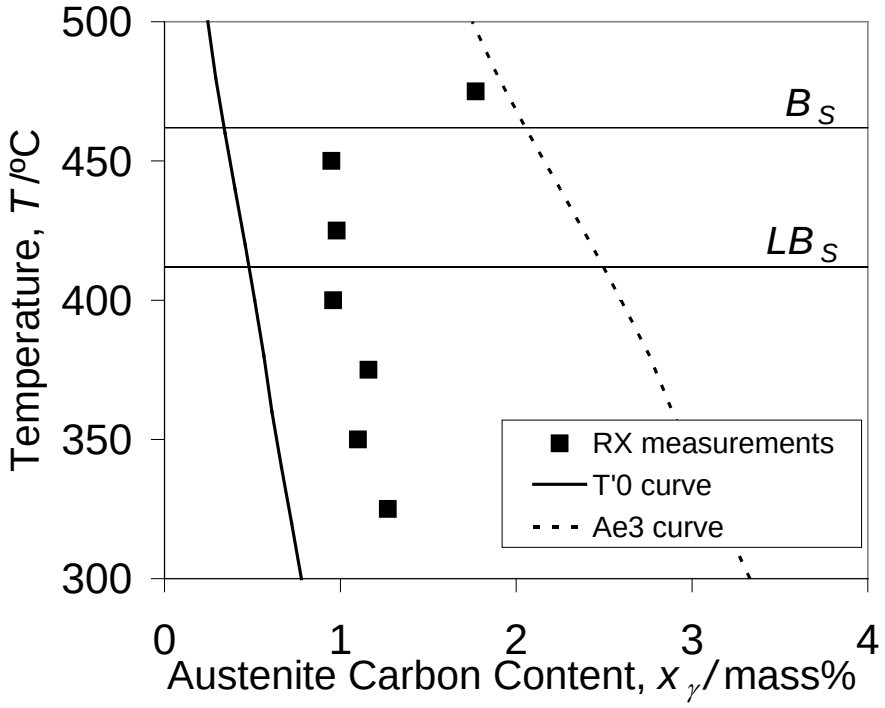

Figure 2 Calculated $T_0^{'}$ and paraequilibrium Ae3 curves[39] for Steel B and experimental data for carbon composition of retained austenite at the termination of bainite and Widmanstätten reactions.

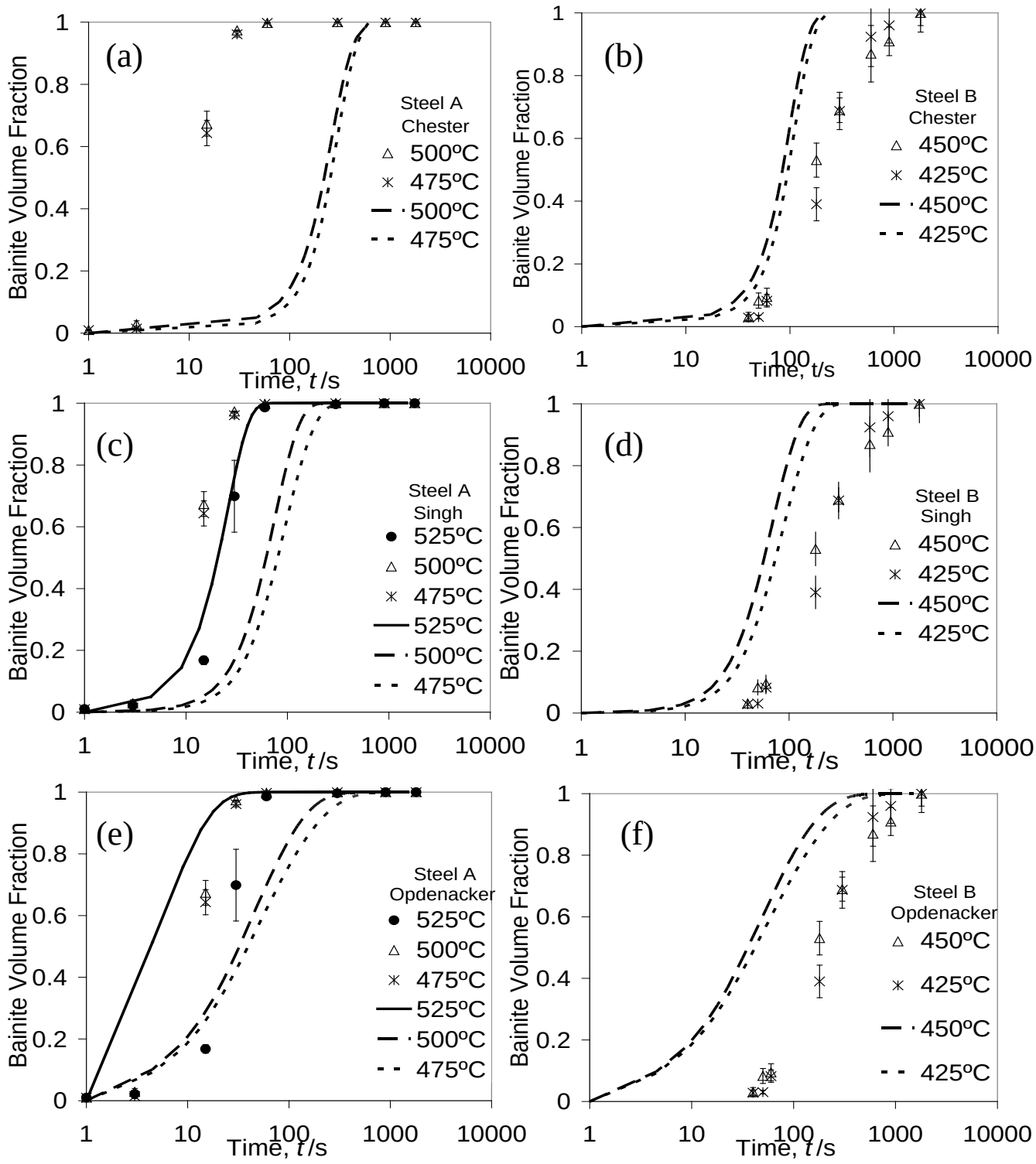

Figure 3 Comparison of experimental and calculated results for the overall transformation kinetics of upper bainite in Steels A and B. eviewed models: a) and b) Chester and Bhadeshia[23] model; c) and d) Singh model[26]; and e) and f) Opdenacker model[29].